ELSEVIER

NeuroImage

www.elsevier.com/locate/ynimg
NeuroImage 23 (2004) 561–568

Detection of diffuse abnormal perfusion in SPECT using a normal brain atlas

Jean-Francois Laliberte,[a] Jean Meunier,[a,*] Max Mignotte,[a] and Jean-Paul Soucy[b]

[a]*DIRO, Departement d'Informatique et de Recherche Operationnelle, University of Montreal, Montreal, Quebec, Canada H3C3J7*
[b]*CHUM (University Hospital), University of Montreal, Montreal, Canada H2L 4M1*

Received 18 December 2003; revised 27 May 2004; accepted 22 June 2004

Visual assessment, with significant inter- or intraobserver variability, is still the norm for the evaluation of Single Photon Emission Computerized Tomography (SPECT) cerebral perfusion studies. We present in this paper an automated method for screening SPECT studies to detect diffuse disseminated abnormalities based on a computerized atlas of normal regional cerebral blood flow (rCBF). To generate the atlas, a set of normal brain SPECT studies are registered together. The atlas contains the intensity mean, the nonlinear displacement mean, and the variance of the activity pattern. A patient is then evaluated by registering his or her SPECT volume to the atlas and computing the nonlinear 3-D displacement of each voxel needed for the best shape fit to it. A voxel is counted as "abnormal" if the intensity difference between the atlas and the registered patient (or if the 3-D motion necessary to move the voxel to its registered position) is superior to 3 SD of normal mean. The number of abnormal voxels is used to classify studies. We validated this approach on 24 SPECT perfusion studies selected visually for having clear diffuse anomalies and 21 normal studies. A Markovian segmentation algorithm is also used to identify the white and gray matters for regional analysis. Based on the number of abnormal voxels, two supervised classifiers were tested: (1) minimum distance-to-mean and (2) Bayesian. The analysis of the intensity and displacement "abnormal" voxels allow one to achieve an 80% correct classification rate for the whole brain and a 93% rate if we consider only voxels in the segmented gray matter region.

Keywords: SPECT; Brain; Atlas; Classification; Optical flow; Segmentation; Markovian segmentation

Introduction

Regional cerebral blood flow distribution has for years been known to be tightly coupled to that of brain glucose and oxygen utilization (McCulloch, 1988). Although this was taken to be coupled to "brain activity," the specific nature of this activity was only more recently shown to be on the level of glutamatergic synaptic transmission, which explains almost all of the consumption of glucose (and therefore of oxygen) in the brain (Sibson et al., 1998). Studies of cerebral blood flow using radioactive tracers in humans were shown to be possible as early as the mid-1960s (Mallet and Veall, 1965), but widespread clinical applications only became possible much later with the introduction of technetium-99m-labeled tracers (e.g., ^{99m}Tc HMPAO or ^{99m}Tc ECD), which show a cerebral distribution that correlated reasonably well with that of perfusion after intravenous administration (Holmes et al., 1985). This distribution can be assessed with Single Photon Emission Computerized Tomography (SPECT), which generates a three dimensional image of the distribution of activity that can then be assimilated to the distribution of cerebral blood flow. SPECT imaging of the distribution of these tracers is now routinely performed in Nuclear Medicine departments, at a fraction of the cost and infrastructure as required by other techniques, that is, positron emission tomography (PET).

Despite the advent of sophisticated image analysis algorithms, most clinical assessments of the normality (or deviation from it) of the distribution of rCBF in SPECT are currently done by visual observation of the studies, searching for side-to-side asymmetries or other "abnormalities" (highly subjective evaluations of the homogeneity of tracer distribution, etc.) in comparison to what could be observed in normals. In fact, in most centers, physicians do not even use a true normal bank of data but rather a more or less informed hypothetical mental construct of what normal studies should look like. Different methods have been described to accurately compare the acquired data with a reference case or series of cases, thereby ensuring more objective identification of regions with modified accumulation of rCBF tracers. Initially, this always implies more or less sophisticated registration algorithms. Once repositioning is performed, numerous techniques have been developed to analyze variations in the distribution of activity of the brain between patients and normals based on predefined statistical criteria, or from one study condition to another in the same subjects.

* Corresponding author. DIRO, Departement d'Informatique et de Recherche Operationnelle, University of Montreal, C.P. 6128 Centre-ville Station, Montreal, Quebec, Canada H3C 3J7. Fax: +1 514 343 5834.
E-mail address: meunier@iro.umontreal.ca (J. Meunier).
Available online on ScienceDirect (www.sciencedirect.com.)

1053-8119/$ - see front matter © 2004 Elsevier Inc. All rights reserved.
doi:10.1016/j.neuroimage.2004.06.029

Although numerous packages have been proposed to accomplish these tasks, one program, Statistical Parametric Mapping (SPM), provided by the Methodology Group at the Wellcome Department of Cognitive Neurology (UK) (SPM, 2004), has been used by significantly more groups than any other. SPM can be applied to SPECT imaging, but in fact its structure makes it either suboptimal or overkill for most SPECT studies. These limitations are in general limited to a much lower number of measurements per subject than those obtained with PET, and even more so with fMRI (Acton and Friston, 1998). Nevertheless, it is possible to use SPM successfully in SPECT under appropriate conditions, at least for research protocols but probably also for everyday clinical work (Ebmeir et al., 2003).

Most of the work in this field has been applied to PET, MRI, and fMRI studies at this time (see Frackowiak et al., 1997; Thatcher et al., 1994; Toga, 1999; Toga and Mazziotta, 2002). Applications in SPECT remain scarce and are not generally available to clinicians, and no consensus exists as to the optimal techniques to be employed. One SPECT study by Houston et al. (1998) is worth noting because our methodology is somewhat related to their work. In their paper, they used a normal SPECT atlas using principal component analysis (PCA) to compare pathological and at-risk groups (boxers, divers with or without decompression illness, subjects with Alzheimer's disease, and schizophrenics). For each group, the percentages of abnormal cortical voxels ($\geq$3 SD of normal atlas activity), and the number of lesions (groups of connected abnormal voxels) were computed and revealed significantly different rCBF patterns between normal controls and that of boxers, divers with decompression illness, and subjects with Alzheimer's disease. Another group (Kovalev et al., 1999; Pagani et al., 2003) has proposed an alternative scheme for SPECT images in Alzheimer's disease (AD) and frontal lobe dementia (FLD). Their algorithm uses a segmented brain atlas to define volumes of interests corresponding to 11 brain regions in the SPECT images. For each region and for the whole brain, they computed approximately one thousand intensity and gradient features. Then, using t statistics, they choose the most appropriate set of features to separate normals, AD and FLD taken two by two. Their method yielded an accuracy of 96.2%, 97.6%, and 94.2% in the separation of AD from normals, FLD from normals, and AD from FLD scans, respectively, using the best set of features in each case. It is important to note that these results were not validated with an independent set of data, and that their percentage values are most probably higher than what could be obtained clinically. Although these results do not represent actual classification rates, they certainly reflect the separability of the classes using their approach.

In this paper, we present and test a method for evaluating SPECT studies based on a computerized atlas of normal regional cerebral blood flow (rCBF). However, its construction neither uses PCA (Houston et al. 1998) nor presegmented anatomical regions (Kovalev et al., 1999; Pagani et al., 2003) but a methodology we have previously developed for MRI anatomical atlas construction (Guimond et al., 1999). This automatic procedure builds a stable average anatomical model of the human brain containing two important features: an average intensity (with the normal variations for each voxel) and an average shape (with the normal shape deformation as an x, y, and z covariance matrix for each voxel). In SPECT imaging, the equivalent atlas will contain not only the normal rCBF (mean intensity and variance, similarly to Houston et al. 1998) for each voxel, but also the extent of possible displacement of the activity pattern (displacement magnitude mean and variance). We expect that the combined activity and displacement information will improve the performance of the detection of anomalies process.

The proposed methodology is optimized for the detection of disseminated diffuse abnormalities, not local or focal ones. Therefore, the precise localization of a particular affected area or the identification of a spatially localized activity pattern is not our main concern here. In clinical practice, diffuse abnormalities are often difficult and tedious to assess because they are barely perceptible and distributed over the whole brain or large areas of it. Our approach can be considered as a screening test to detect such diffuse abnormalities. It is implied that a nuclear physician will subsequently further investigate (and classify, if possible, as suggestive of a specific process) the detected abnormal cases.

Materials and methods

Two main operations are needed using our strategy to detect abnormal perfusion patterns in SPECT. The first one is the construction of an atlas of the normal brain of the type described above, and the second one is the application of an objective criterion to classify a patient as normal or abnormal by comparing his or her SPECT study to the atlas. We also evaluated whether classification could be improved by limiting the analysis to only a portion of the data, that is, cortical voxels.

Atlas construction

Creation of the atlas requires several normal SPECT studies that must be registered into a unique reference volume. We first normalize the intensity of all studies to account for different parameters (see below) that are not directly related to diffuse perfusion abnormalities. Then the SPECT volumes are coregistered using a linear transformation to make all brains comparable in size and orientation. Finally, we compute the individual SPECT pattern shape differences, yielding displacement mean and variance, which will be incorporated in the atlas along with the intensity mean and variance. We now describe the methodology in more detail.

Intensity normalization

The registration algorithm assumes the same intensity for corresponding brain structures in the two images to be aligned. This assumption is rendered unrealistic by multiple factors, such as acquisition parameters (administered dose, camera performance, etc.), subjects' body conformation, or variations in pre- and postprocessing of data. To correct for these nonrelevant differences in signal intensity, a linear correction is used. Assuming an initial rough registration of the two brain images, a joint histogram is computed. The slope of the line of a linear regression through this histogram gives the multiplication factor to compensate for the overall intensity difference (Fig. 1). To fit the line, we use a very simple procedure that looks for a regression line going through the origin and dividing the set of points in Fig. 1c (joint histogram) in two equal sets. This algorithm offers robustness to outliers by computing a median line and is very simple to implement. To increase the reliability of results, this evaluation is repeated before the nonlinear registration (often with no or almost no change).

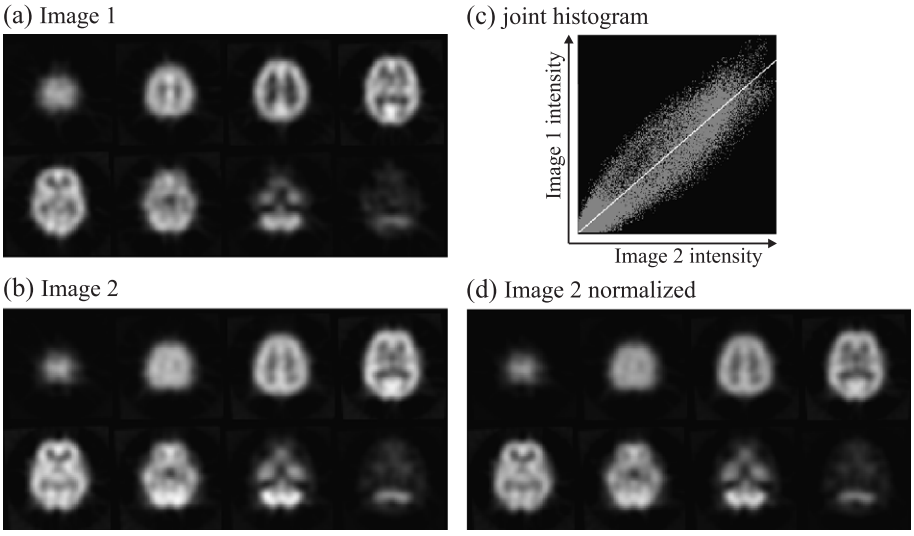

Fig. 1. Image normalization.

Linear registration

A 3-D image sequence (of two or more images) can be mathematically described as a function $I(x,y,z,t)$ where I is the image intensity at time t and position (x,y,z). Using the chain rule for derivatives, one obtains the basic constraint of optical flow (Horn and Schunck, 1981):

$$\frac{dI}{dt} = \frac{\partial I}{\partial x}U + \frac{\partial I}{\partial y}V + \frac{\partial I}{\partial z}W + \frac{\partial I}{\partial t} \tag{1}$$

The partial derivatives can be estimated directly from the two SPECT images to be coregistered. The four remaining variables $U = dx / dt$, $V = dy / dt$, $W = dz / dt$, and dI / dt represent the motion (velocity) along the x, y, and z axes and the object (here, brain) brightness changes, respectively. This equation lays down a first constraint to determine the motion (registration) between two SPECT images. The linearity condition provides another constraint:

$$\begin{bmatrix} U \\ V \\ W \end{bmatrix} = \vec{T} + \mathbf{M}\begin{bmatrix} x \\ y \\ z \end{bmatrix} \tag{2}$$

where $\vec{T}$ is a translation vector and $\mathbf{M}$ is a 3×3 general matrix. $\mathbf{M}$ can therefore incorporate rotation and scaling as well as shearing. Eq. (2) represents an affine (or linear) transformation. A last constraint is used to model the behavior of the change in brightness dI / dt. One option is to set dI / dt to 0, which means no change in object (brain) intensity (Horn and Schunck, 1981). This constraint is assumed valid when the brain SPECT images are first intensity normalized as described in the previous section.

The overdetermined system obtained by writing down the basic optical flow equation using the linearity and dI / dt constraints for each voxel can be solved as a least square problem using the corresponding normal equations. In this way, one obtains the linear field transformation needed to align both brain SPECT volumes and to give them the same size and orientation. This approach can be used iteratively by keeping track of intermediate results (Barber, 1992, 1995) to improve the results when the two brains "start" from very different orientations in the original images.

One should note that in general, to ensure robustness, a good preregistration is necessary to initialize the optical flow linear registration. For this purpose, we use the theoretical model of Alpert et al. (1990). We first set a threshold at 25% of the maximum activity to get two brain masks. Then a principal component analysis (PCA) is done on the mask voxel x, y, and z coordinates to extract the main axes and the centers of gravity. The registration of the centers of gravity and main axes gives the 3-D translation and rotation needed for preregistration. A crude scaling factor is also computed by comparing the volume (number of voxels) of each mask. The resulting final transformation is composed of a 3-D translation, a 3-D rotation, and an isotropic scaling factor and is used to preregister the SPECT images.

Nonlinear registration

We used the algorithm developed by Horn and Schunck (1981) to compute the nonlinear residual transformation used to refine the coregistration of both volumes. The algorithm initially computes the x, y, and z motions U, V, and W using the optical flow brightness constraint (Eq. (1)) to get an initial solution (motion component perpendicular to the gray-level isocontours):

$$U = -\frac{\partial I}{\partial x}\frac{\partial I/\partial t}{\| \nabla I \|^2 + \alpha^2} \quad V = -\frac{\partial I}{\partial y}\frac{\partial I/\partial t}{\| \nabla I \|^2 + \alpha^2}$$
$$W = -\frac{\partial I}{\partial z}\frac{\partial I/\partial t}{\| \nabla I \|^2 + \alpha^2} \tag{3}$$

Subsequently, the optical flow (U, V, and W) is iteratively smoothed (local average) and then updated to the nearest solution of the brightness constraint equation:

$$U^{k+1} = \bar{U}^k - \frac{\partial I}{\partial x}\frac{\nabla I \cdot (\bar{U}^k, \bar{V}^k, \bar{W}^k) + \partial I/\partial t}{\| \nabla I \|^2 + \alpha^2}$$

$$V^{k+1} = \bar{V}^k - \frac{\partial I}{\partial y}\frac{\nabla I \cdot (\bar{U}^k, \bar{V}^k, \bar{W}^k) + \partial I/\partial t}{\| \nabla I \|^2 + \alpha^2}$$

$$W^{k+1} = \bar{W}^k - \frac{\partial I}{\partial z}\frac{\nabla I \cdot (\bar{U}^k, \bar{V}^k, \bar{W}^k) + \partial I/\partial t}{\| \nabla I \|^2 + \alpha^2} \quad (4)$$

where the bar over $\bar{U}^k$ represents the local average (using a $3 \times 3 \times 3$ mean filter) at the kth iteration. The α^2 term helps to avoid unreliable results introduced by low values of $||\nabla I||$. This also ensures that high contrast contours will drive the nonlinear warping and prevents small interpatient brightness differences (small $||\nabla I||$) from inappropriately affecting the warping process. Moreover, the larger α is, the smoother the nonlinear transformation will be (Horn and Schunck, 1981). In this study, we found after several tests that a (large) α value of 100 was a good choice for the type of task at hand (see below). The resulting nonlinear field is smooth and allows a good coregistration of the two SPECT volumes. Do note that it can only be used following a prior linear registration step, otherwise the spatial and temporal derivatives risk becoming too unreliable.

Atlas construction principles

The actual construction of the atlas can begin as schematically illustrated in Fig. 2 after linear volume registration and intensity correction of all normal brains to be incorporated into the atlas (also see Appendix A for details).

First, we select a brain amongst the normal ones to be used as a reference (black square in Fig. 2). We then coregister the other ones (white squares) to this reference using the nonlinear optical flow procedure described in the previous section. At this point, the intensity mean and variance can be computed. However, since the reference brain is chosen arbitrarily, it cannot be considered to represent any "absolute" normalcy of shape. Therefore, the mean displacement needed to coregister the normal brains is calculated and subtracted from all brains to obtain the average brain shape in addition to the average intensity (gray square). The final atlas consists of the normal average and variance of the intensity and displacement of the SPECT activity pattern.

Classification

Evaluation of any given patient proceeds in a manner similar to that used for constructing the atlas. We begin by registering the patient's SPECT volume to the atlas (average brain intensity and shape) with a linear intensity correction and an affine transformation, following the procedure described in the linear registration section. The algorithm computes the nonlinear 3-D displacement of each voxel needed for an almost perfect shape fit with the atlas (nonlinear registration section).

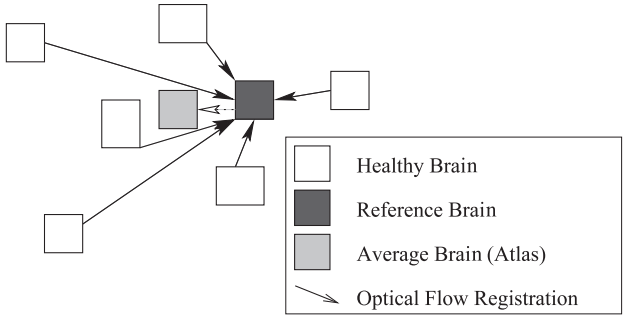

Fig. 2. Atlas construction.

For each patient's brain voxel, we can then compare the intensity and nonlinear displacement to their normal values in the reference system of the atlas. To reduce the dimensionality of the problem, we consider only the number of abnormal voxels for intensity and the number of abnormal voxels for displacement as the two new attributes for classification. Assuming a Gaussian probability density function (PDF) for the intensity, a voxel is assumed to be abnormal if its intensity is more than 3 SD above or under the atlas mean. Assuming a Rayleigh PDF for the displacement, a voxel is assumed to be abnormal if the corresponding displacement is more than 3 SD above the atlas mean (note that a Rayleigh distribution implies that abnormal values are higher than the mean).

Obviously, we expect normal individuals to show relatively small numbers of outliers while the reverse would be observed in patients with abnormal brain perfusion. To classify normal and abnormal brains, we tested two quite simple classifiers. The first one is a minimal distance classifier in which one counts the number of outliers and places the patient in the class with the nearest mean number of outliers. The other one is the Bayes classifier, which assigns the subject to the most likely class assuming a Gaussian PDF model for each class (Duda et al., 2000).

The different steps involved in our algorithm can be summarized as follows:

Atlas creation steps:

1. Gross alignment of each normal subject on a target brain
2. Intensity normalization of each subject with the target brain
3. Spatial registration to the target brain with an affine transformation
4. Second intensity normalization
5. Non linear registration to the target brain
6. Subtraction of the average (nonlinear) displacement from all brains
7. Final construction of the atlas, which consists for each voxel of:
   a. mean and variance of the intensity
   b. mean and variance of the displacement for the set of all registered brains of the previous step.

Detection steps:

1. Gross alignment of the tested subject with the atlas intensity mean
2. Intensity normalization of the tested subject with the atlas
3. Spatial normalization to the atlas with an affine transformation
4. Second intensity normalization
5. Non linear registration to the atlas
6. Counting of the number of outliers (abnormal voxels)
7. Decision

Region of interest (ROI) segmentation

One could be interested in investigating the values of the attributes used here for classification in a specific region of interest (ROI) of the brain. For instance, since we are evaluating perfusion anomalies that might preferentially occur in a specific compartment, such as the gray matter, we wanted to ascertain whether concentrating on cortical structures might improve segregation of abnormal cases. In SPECT imaging, identification of the whole brain can generally be done quite satisfactorily by choosing a threshold of 25% of the maximum number of counts (or gray level), eventually with some preprocessing. However, for gray

matter segmentation, a threshold approach will not be efficient because too many voxels in the gray matter have intensity values that overlap with those of the white matter. To solve this problem, we used an unsupervised Markovian segmentation algorithm that we have already presented elsewhere (Mignotte and Meunier, 2000; Mignotte et al., 2002), which is able to discriminate automatically between white and gray matter. Briefly, the algorithm tries to classify a voxel as white or gray matter according to its intensity and the class of its neighbors. This can be mathematically formulated as follows:

$$\arg\min_{c} \sum_{x,y,z} \left(-\ln P\left(I_{x,y,z} \mid c_{x,y,z}\right) + \sum_{\substack{neighbors \\ of\ x,y,z}} \left(1 - \delta\left(c_{x,\,y,\,z},\, c_{\text{neighbors}}\right)\right) \right) \tag{5}$$

The tissue class $c_{x,y,z}$ represents one of the three brain structures that are white matter, gray matter, and CSF/background. The probability density function $P(I_{x,y,z}|c_{x,y,z})$ gives for each class $c_{x,y,z}$ the corresponding PDF of the intensity $I_{x,y,z}$ for a voxel (x,y,z). The first term is thus proportional to the likelihood of having a particular intensity for a given class. For instance, if a voxel is relatively bright, its likelihood of being in class "gray matter" will be higher. To favor homogeneous regions a second term is added. This summation is taken over all pairs of voxels consisting of the current voxel (x,y,z) and one of the voxels in the six-voxel neighborhood (left, right, above, under, behind, or in front). If the class of the neighbor is the same, then $\delta(c_{x,y,z}, c_{\text{neighbors}})$ equals 1, otherwise it equals 0. Therefore, when the segmentation is good, the classes are correctly assigned and $P(I_{x,y,z}|c_{x,y,z})$ is relatively high and consequently the first term is low (due to the minus sign). Moreover, the second term is also small since the regions are homogeneous. The segmentation problem becomes a minimization problem for which we look for the best labeling of the voxel, that is, the one that minimizes the terms within bracket. Notice that to solve this problem, we need to assess the PDF of the intensity for each class. For this purpose, we fitted an exponential law for the "CSF/background" area, and two different Gaussian laws for the "white matter" and the "gray matter" regions; together, these distributions approximate very well the intensity histogram of the SPECT image governed by Poisson processes. The estimation algorithm for the PDF parameters as well as the optimization details can be found in Mignotte and Meunier, (2000) and Mignotte et al. (2002).

Results

Data set

We validated this approach using 24 SPECT brain perfusion studies (^{99m}Tc ECD) selected because they visually showed undeniable diffuse anomalies, which were expected given the clinical information available. The detection of abnormal diffuse perfusion is typically a difficult task and is certainly much more challenging than focal lesions detection. The atlas was constructed with 21 perfusion studies from normal volunteers (hospital employees, residents, and physicians). Care was taken to keep the acquisition and image reconstruction protocols as constant as possible [e.g., sampling, levels of statistics (counts), filtering, reconstruction, and restoration methods] for all studies. Each transversal slice contains 64 × 64 pixels and there are typically around 40 slices per individual. The number of counts are rescaled for 8 bits/pixel (256 gray levels). The volume was padded with additional slices to get a set of uniform dimension volumes (64 × 64 × 64 voxels with isotropic dimensions of 4.2 millimeters/voxel).

Atlas construction

Fig. 3 shows the behavior of the registration process used in the atlas construction with image differences and mosaics. In Fig. 3a, the difference between corresponding transaxial slices from two different brains shows the initial misalignment clearly (black, gray, and white corresponding to negative, no, and positive differences, respectively). After linear normalization for brain size and orientation (Fig. 3c), the difference decreases considerably but not completely. This was expected since some groups (Evans et al., 1991; Strother et al., 1994) have shown in MRI that linear models will leave a residual root means square mismatch of 6–7 mm. Finally, Fig. 3e presents the typical intensity differences that will be kept in the atlas after nonlinear registration. Figs. 3b, d, and f display the same results as mosaics of 5 × 5 pixels squares of each image appearing in turn to help assess the registration process. Fig. 4 shows the normal SPECT rCBF atlas using gray level images. It contains four kinds of information: (a) the intensity average, (b) the displacement magnitude average, (c) the intensity variance, and (d) the displacement variance. All images were normalized for display purposes. The original range of values is given in the figure caption.

Validation

Due to the small data set, a leave-one-out strategy (Bishop, 1994) was used to test our approach to avoid any bias (Fig. 5). Essentially this means that in turn, one perfusion study is used to test the algorithm while the other ones are used for the atlas construction and classifier parameter estimation.

Table 1 shows the success rates for both classifiers using the number of intensity outliers only, the number of displacement outliers only, or both attributes for classification. Since we are particularly interested in abnormal diffuse perfusion that typically occurs in the gray matter, Table 2 displays the success rates when only voxels from that compartment are considered. In each table, one observes that the best results are obtained with the Bayes classifier using both attributes, and as expected, the gray-matter-only classification shows the best performance (93.3% vs. 80%). However, the confidence intervals are often large due to the small number of SPECT studies available (total: 45), and therefore it is difficult to conclude as to the definitive superiority of the gray-matter-only Bayes algorithm over all the other methods.

Conclusion

We have presented a method to detect diffuse brain anomalies in SPECT that uses a normal rCBF numerical atlas containing for each voxel both the normal rCBF (mean intensity and variance) and the displacement of the activity pattern (as displacement mean and variance). We have then successfully tested this atlas for the detection of diffuse rCBF disorders with simple classification algorithms after dimensionality reduction. To our

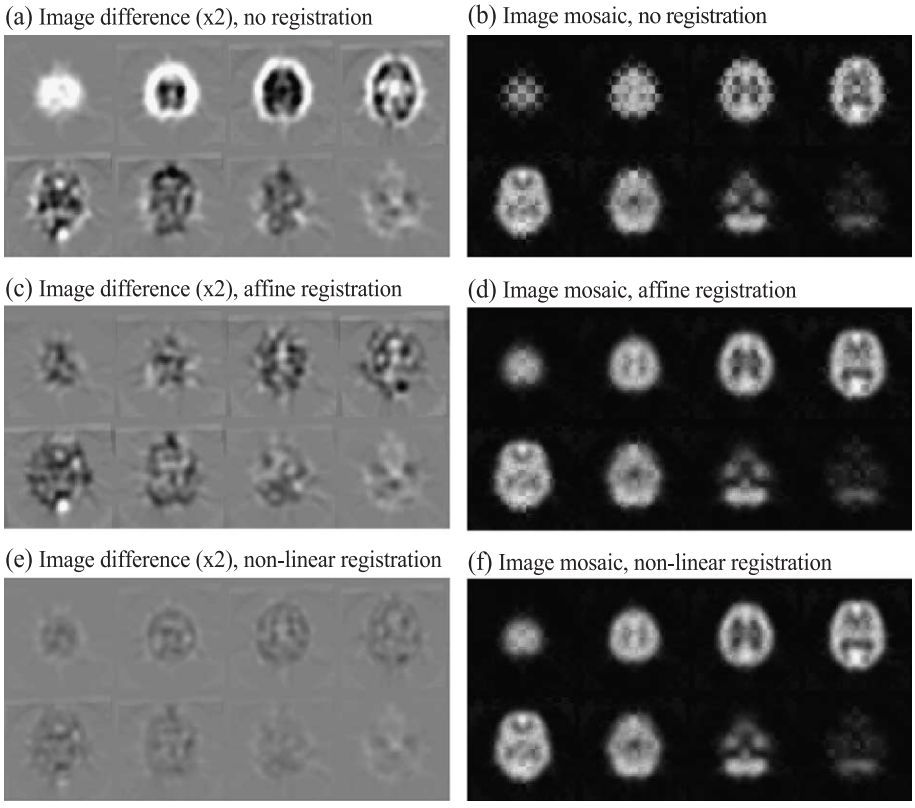

Fig. 3. Registration process behavior for different approach.

knowledge, there is no other simple and automatic method, based on a statistical atlas, to carry out such a complex interpretation task (detection of diffuse anomalies in SPECT) with a success rate higher than 90% (with an independent data set or cross validation) as obtained in this work. However, we recognize that the good success rates obtained in this work cannot be considered to be definitive, as the number of SPECT studies is rather limited. We therefore intend to test this approach on a larger number of cases with different and more specific disorders in both SPECT and PET.

Focal or local abnormalities were not considered here. Although our method could detect focal abnormalities, it was not designed for such a task. Indeed, these abnormalities are often easier to localize in practice by comparing (visually or automatically) the left and right hemisphere for instance.

Although registration of the SPECT images within one of the standard frames of reference for brain imaging (e.g., Talairach and Tournoux, 1988, or MNI152 SPM, 2004) could be possible, it was not necessary for our purpose since we do not need to localize abnormalities. Moreover, these systems suffer from some draw-

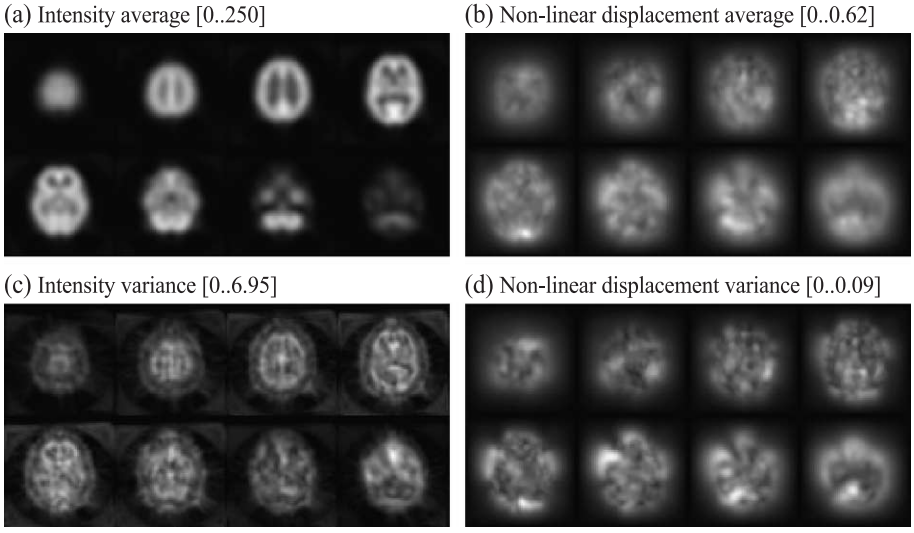

Fig. 4. Atlas features.

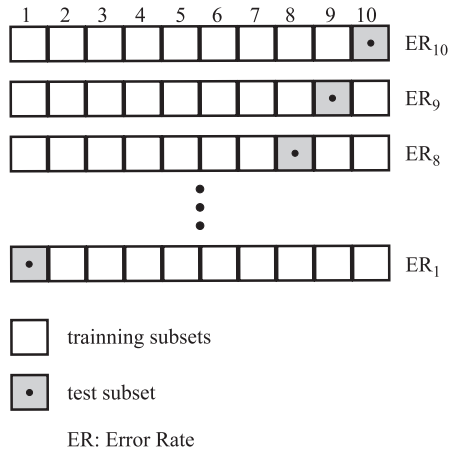

Fig. 5. The leave-one-out process divides a set in multiple subsets and alternately evaluates the Error Rate (ER) for each subset. The average $(\frac{1}{n}\sum_{i=0}^{n} \mathrm{ER}_i)$ gives a better estimation of the algorithm performance (ER).

backs. For instance, the Talairach atlas is based on one 60-year-old postmortem individual that is not necessarily representative of any given population. It is well known that brain variability increases with the distance from the main axis (the AC-PC line). The current standard MNI template (MNI152) is the average of 152 normal MRI scans registered in the Talairach space. However, the matching transformations used to construct this atlas were strictly linear (nine parameters). For these reasons, and although registration of the SPECT images within one of these spaces remains possible, we decided to construct a representative atlas of the SPECT rCBF directly from our data set.

As stated previously, most of the work in neurofunctional imaging has been applied to PET, MRI (morphometry), and fMRI studies at this time, but several problems are similar in SPECT. Unfortunately, applications in SPECT remain scarce mainly because SPECT is often (we believe) underestimated. SPECT has drawbacks with respect to PET and fMRI/MRI (e.g., lower resolution and no absolute rCBF value), but this is rapidly improving with better radionuclide tracers and higher resolution [see for instance the NeuroFOCUS (NeuroPhysics, 2004) system, with a 3-mm resolution]. It also has several other advantages, such as a much lower cost and wider availability than that of PET or fMRI. In addition, out-of-scanner radionuclide injections are possible with SPECT, and this still represents the only applicable technique for research purposes in cerebral function mapping for tasks where a subject cannot be placed in a fMRI magnet or PET camera (complex protocols with patient motion, metallic instrumentation, ictal monitoring of epilepsy patients, etc.).

Our goal was to develop an automatic algorithm for the screening of brain rCBF SPECT studies for the detection of diffuse abnormalities. We believe that in clinical practice, such a tool will significantly reduce the burden of visually assessing rCBF studies. Moreover, such methodology could certainly be applied in several other types of studies in SPECT as well as in PET, fMRI, and other imaging modalities where atlas construction is applicable.

Table 1
Whole brain classification results

	Classification success rate, *n* (%)	Confidence interval 95% [%–%]	False positive, *n* (%)	False negative, *n* (%)
Minimal distance classifier				
Intensity	30 (66.7)	[52.1–78.6]	11 (24.4)	4 (8.9)
Pattern displacement	36 (80.0)	[66.2–89.1]	6 (13.3)	3 (6.7)
Both	35 (77.8)	[63.7–87.5]	7 (15.6)	3 (6.7)
Bayes classifier				
Intensity	31 (66.7)	[54.3–80.5]	10 (22.2)	4 (8.9)
Pattern displacement	35 (77.8)	[63.7–87.5]	7 (15.6)	3 (6.7)
Both	36 (80.0)	[66.2–89.1]	6 (13.3)	3 (6.7)

Table 2
Gray matter only classification results

	Classification success rate, *n* (%)	Confidence interval 95% [%–%]	False positive, *n* (%)	False negative, *n* (%)
Minimal distance classifier				
Intensity	33 (73.3)	[59.0–84.0]	9 (20.0)	3 (6.7)
Pattern displacement	37 (82.2)	[68.7–90.7]	7 (15.6)	1 (2.2)
Both	40 (88.9)	[76.5–95.2]	4 (8.9)	1 (2.2)
Bayes classifier				
Intensity	42 (93.3)	[82.1–97.7]	1 (2.2)	2 (4.4)
Pattern displacement	40 (88.9)	[76.5–95.2]	3 (6.7)	2 (4.4)
Both	42 (93.3)	[82.1–97.7]	1 (2.2)	2 (4.4)

Acknowledgments

This research was supported by the Natural Sciences and Engineering Research Council of Canada (NSERC) and the Fonds Nature et Technologies du Québec (NATEQ).

Appendix A. Atlas creation at the voxel level

The atlas construction principles are described in Materials and methods. In this appendix, we explain in more details the creation of the atlas and in particular the resampling methodology needed for that purpose. Fig. 6 illustrates the methodology in 2-D for easier display, but the same principles apply in 3-D. First, we select a brain amongst the normal ones to be used as a reference. Fig. 6a represents four centers of voxel (black disks: ●) of that brain. We then coregister the other normal brains to this reference using the nonlinear optical flow procedure described in Materials and methods. The computed displacement vectors are displayed in Fig. 6a for three different normal brains with an indication for each reference voxel the corresponding voxel in the three other normal brains. Since the reference brain is chosen arbitrarily, it cannot be considered to represent any "absolute" normalcy of shape. Therefore, the mean displacement is calculated and subtracted from the reference brain to obtain the average brain shape and intensity. Fig. 6b shows the average displacement vectors for each reference voxel. To remove the average displacement from the reference brain, we must deform it according to the average displacement field. This means that positions identified by a circle (○) in Fig. 6c

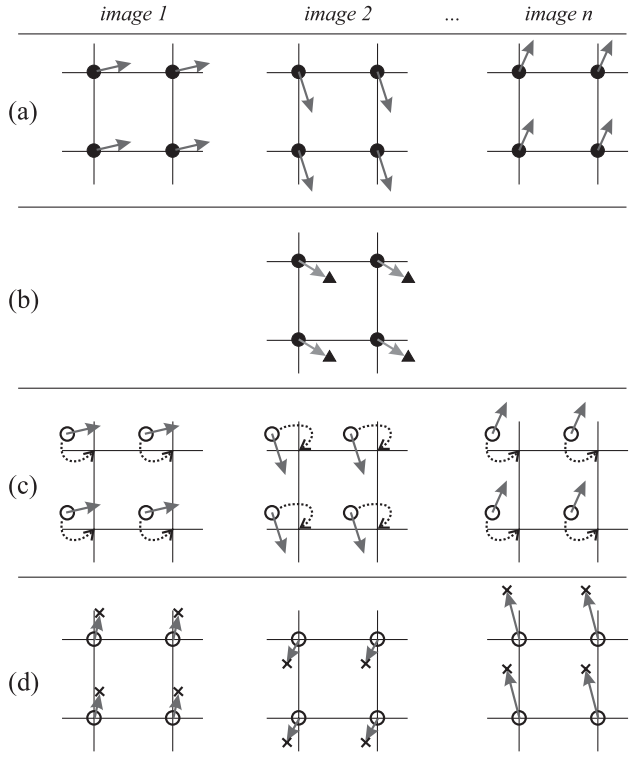

Fig. 6. Resampling methodology for atlas construction (see text).

will move to the integer coordinates of the voxel centers while the original voxel centers will move to positions identified by a triangle (▲) (Fig. 6b) after the transformation. To obtain the final normal displacement at the center of each voxel, we therefore interpolate (trilinear interpolation of each x, y, and z component of the vector) the displacement vectors for each circle (○) and subtract the mean displacement (Fig. 6d). The final displacement atlas consists of the average length (and variance) of these (corrected) vectors. The corresponding final intensity atlas consists of the average and variance of the interpolated intensity (3-D cubic interpolation; Wolberg, 1990) at the tip of the displacement vectors (marked with × in Fig. 6d) in each original normal brain images.

References

Acton, P.D., Friston, K.J., 1998. Statistical Parametric Mapping in functional neuroimaging: beyond PET and fMRI activation studies. Eur. J. Nucl. Med. 25 (7), 663–667.

Alpert, N.M., Bradshaw, J.F., Kennedy, D., Correia, J.A., 1990. The principal axes transformation, a method for image registration. J. Nucl. Med. 9, 1717–1722.

Barber, D., 1992. Registration of low resolution medical images. Phys. Med. Biol. 37 (7), 1485–1498.

Barber, D., Tindale, W., Hunt, E., Mayes, A., Sagar, H., 1995. Automatic registration of SPECT images as an alternative to immobilization in neuroactivation studies. Phys. Med. Biol. 40 (3), 449–463.

Bishop, C., 1994. Neural Network for Pattern Recognition. Oxford Univ. Press, New-York.

Duda, R., Hart, P., Stork, D., 2000. Pattern Classification, second ed. Wiley-Interscience Publication, New York.

Ebmeier, K.P., Darcourt, J., Dougall, N.J., Glabus, M.F., Herholz, K., Koulibaly, P.M., Migneco, O., Nobili, F., Pupi, A., Robert, P., Rodriguez, G., Scheidhauer, K., 2003. Voxel-based approaches in clinical imaging. SPECT in dementia. In: Ebmeier, K.P. (Ed.), Advances in Biological Psychiatry. S. Karger Publishing, Basel, Switzerland, pp. 72–85.

Evans, A., Dai, W., Collins, L., Neelin, P., Marrett, S., 1991. Warping of a computerized 3-D atlas to match brain image volumes for quantitative neuroanatomical and functional analysis. Proc. Int. Soc. Opt. Eng.: Med. Imaging 1445, 236–247.

Frackowiak, R.S.J., Friston, K.J., Frith, C.D., Dolan, R.J., Mazziotta, J.C., 1997. Human Brain Function. Academic Press, San Diego.

Guimond, A., Meunier, J., Thirion, J.-P., 1999. Average brain models: a convergence study. Comput. Vis. Image Underst. 77 (2), 192–210.

Holmes, R.A., Chaplin, S.B., Royston, K.G., Hoffman, T.J., Volkert, W.A., Nowtnik, D.P., Canning, L.R., Cumming, S.A., Harrison, R.C., Nechvatal, H.G., Pickett, R.D., Piper, I.M., Neirinckx, R.D., 1985. Cerebral uptake and retention of ^{99m}Tc-hexamethylpropylene amine oxime (^{99m}Tc-HM-PAO). Nucl. Med. Commun. 6, 443–447.

Horn, B.K.P., Schunck, B.G., 1981. Determining optical flow. Artif. Intell. 17, 185–204.

Houston, A.S., Kemp, P.M., Macleod, M.A., Francis, J.R., Colohan, H.A., Matthews, H.P., 1998. Use of significance image to determine patterns of cortical blood flow abnormality in pathological and at-risk groups. J. Nucl. Med. 39 (3), 425–430.

Kovalev, V., Thurfjell, L., Lundqvist, R., Pagani, M., 1999. Classification of SPECT scans of Alzheimer's disease and frontal lobe dementia based on intensity and gradient information. Med. Image Understand. Anal. 19–20, 69–72.

Mallet, B.L., Veall, N., 1965. The measurement of regional cerebral clearance rates in man using Xenon-133 inhalation and extracranial recordings. Clin. Sci. 29, 179–191.

McCulloch, J., 1988. The physiology and regulation of cerebral blood flow. In: Knezevic, S., Maximillian, V.A., Mubrin, Z., Prohovnik, I., Wade, J. (Eds.), Handbook of Regional Cerebral Blood Flow. Lawrence Erlbaum Associates, Mahwah, NJ, pp. 1–24.

Mignotte, M., Meunier, J., 2000. Three-dimensional blind deconvolution of spect images. IEEE Trans. Biomed. 47 (2), 274–281.

Mignotte, M., Meunier, J., Soucy, J., Janicki, C., 2002. Comparison of deconvolution techniques using a distribution mixture parameter estimation: application in spect imagery. J. Electron. Imaging 11 (1), 11–25.

NeuroPhysics, 2004. NeuroPhysics Corporation. Available at http://neurophysics.com/index.html.

Pagani, M., Kovalev, V., Lundqvist, R., Jacobssen, H., Larsson, S., Thurfjell, L., 2003. A new approach for improving diagnostic accuracy in Alzheimer's disease and frontal lobe dementia utilising the intrinsic properties of the SPET dataset. Eur. J. Nucl. Med. Mol. Imaging 30 (11), 1481–1488.

Sibson, N.R., Dhankhar, A., Mason, G.F., Rothman, D.L., Behar, K.L., Shulman, R.G., 1998. Stoichiometric coupling of brain glucose metabolism and glutamatergic neuronal activity. Proc. Nat. Acad. Sci. 95, 316–321.

SPM Central, 2004. Statistical Parametric Mapping. Available at http://www.fil.ion.ucl.ac.uk/spm.

Strother, S., Anderson, J., Xu, X., Liow, J., Bonar, D., Rottenberg, D., 1994. Quantitative comparisons of image registration technique based on high resolution MRI of the brain. J. Comput. Assist. Tomogr. 18 (6), 954–962.

Talairach, J., Tournoux, P., 1988. Co-planar Stereotaxic Atlas of the Human Brain: 3-Dimensional Proportional System—An Approach to Cerebral Imaging. Thieme Medical Publishers, New York.

Thatcher, R.W., Hallett, M., Zeffiro, T., John, E.R., Huerta, M., 1994. Functional Neuroimaging, Technical Foundations. San Diego: Academic Press.

Toga, W.T., 1999. Brain Warping. Academic Press, San Diego.

Toga, W.T., Mazziotta, J.C., 2002. Brain Mapping The Methods, second ed. Academic Press, San Diego.

Wolberg, G., 1990. Digital Image Warping. IEEE Computer Society Press, Los Alamitos, CA, pp. 124–161.